# Dissolution Kinetics of Synthetic Amorphous Silica in Biological-Like Media and Its Theoretical Description

**Frank Roelofs* and Wolfram Vogelsberger**

*Institute of Physical Chemistry, Chemistry and Earth Science Faculty, Friedrich-Schiller-University Jena, Lessingstrasse 10, D-07743 Jena, Germany*

*Received: March 19, 2004; In Final Form: May 13, 2004*

Different types of synthetic amorphous silica have been dissolved under biological-like conditions in a buffer system. The buffer solution named TRIS buffer provides a system with comparable pH value, buffer capacity, and osmotic pressure as it can be found in extracellular fluid. Additionally, the phospholipid L-α-dipalmitoylphosphatidylcholine (DPPC) has been used in several dissolution experiments to simulate conditions which are found in extracellular lung fluid. The molybdic acid method (used as standard procedure) and partly ICP−OES have been applied to determine the total amount of silica dissolved. The dissolution of nanodisperse silica shows a strong size effect, which leads to a significant higher silica concentration when compared with the bulk phase. At longer dissolution time a slight decrease of solubility can be observed. The Gibbs free energy of cluster formation is calculated numerically for the dissolution process to predict the temporal development of silica concentration. Theoretical curves are adapted by nonlinear regression of a free parameter. This parameter can be understood as the rate constant of the dissolution process.

## 1. Introduction

Nanodisperse substances like silica are employed in a wide range of technical applications. They are often used in the form of their colloidal dispersion. In general, such nanoparticles have a low solubility in solvents such as water. But due to the increased energy of these particles when compared with the bulk phase, they exhibit special properties. For example, small particles show a noticeable increased solubility. Such kind of particles (often fine powders) can easily be inhaled during the contact. A number of publications exist in the literature dealing mainly with the dissolution behavior of glass or mineral fibers in simulated lung fluid.[1−3] These experiments were carried out under dynamic conditions with different flow rates. Icenhower et al.[4] investigated the dissolution rates of special amorphous silica with very low surface areas at 40 to 250 °C. These investigations were carried out at different NaCl concentration. In conclusion, they have calculated overall rate constants, $k_+$, of the dissolution process. Further on, Vogelsberger et al.[5] proposed a kinetic model for the solubility of oxidic solids in water by applying a set of elementary reactions. The overall rate constant of the dissolution process has been determined for the dissolution of silica gels. Very interesting investigations were done by House et al.[6] and Zhmud et al.[7] determining rate constants for the release of dissolved silica from different (river) sediments. The experiments were carried out under close to natural conditions at lower temperatures and at approximately neutral pH with a circulated overlying solution. In the present investigations, we have studied the dissolution behavior of synthetic amorphous silica with high specific surface areas in systems with biological-like properties and under static conditions. So, we can determine rate constants by applying kinetic and thermodynamic considerations. The dissolution process was carried out in TRIS buffer at 37 °C. This buffer solution provides the mentioned conditions. The special conditions in biological lung fluid requires the consideration of surface-active components. Proper lung function requires a low surface tension to minimize the work of breathing and to ensure uniform lung inflation.[8] The complex mixture of the lung surfactant is specified with slight differences in the literature. The main part of this surfactant has been identified as phospholipids[9−14] with a different ratio (*x*:*y*) of chain length of the fatty acid (*x*) to number of double bonds (*y*). The predominant (approximately 80%) and most surface active component of this part is L-α-dipalmitoylphosphatidylcholine (DPPC), a 16:0 phospholipid.[9,11−14] For a very simple model system, DPPC was added to the dissolution experiments to study the possible influence of the surfactant on the dissolution behavior.

The dissolution kinetics was observed by measuring the actual amount of silica dissolved. Additionally, we measured the pH value and carried out surface characterization by nitrogen adsorption measurements to observe changes in the surface morphology. Further on, dynamic light scattering measurements were carried out to investigate the goodness of surfactant dispersions and to try to determine the changes in the particle radius distribution of undissolved silica directly during the dissolution process.

The results were interpreted using a model described earlier,[15] which calculates the Gibbs free energy as the natural thermodynamic potential for these cases. It considers the presence of a colloid forming species, solute, and an inert solvent. The model involves nucleation (particle growth), Ostwald ripening, and particle dissolution in an uniform description. The gradient of the Gibbs free energy operates as the driving force for the changes in the system, here. A simple approach for the rate law is chosen to describe the change in the dissolution process over time. We obtain the rate constant of the dissolution process as the only parameter by fitting this theoretical model to our experimental data by nonlinear regression.

* Corresponding author. Telephone: +49 3641 948347. Fax: +49 3641 948302. E-mail: Frank.Roelofs@uni-jena.de.

10.1021/jp048767r CCC: $27.50 
Published on Web 07/03/2004

**TABLE 1: Overview of the Dissolution Important Properties of Silicas Used (Specific Surface Area, $S_{BET}$, and Primary Particle Radius, $r_p^{avg}$) and the Measured Quantities of the Dissolution Experiments**

| | silica samples | | properties | | experimental data and quantities | | | | |
|---|---|---|---|---|---|---|---|---|---|
| expt | name | produced by | $S_{BET}$ ($m^2/g$) | $r_p^{avg}$ (nm) | pH | $m_s$ (g) | $V_L$ (mL) | solvent | surfactant |
| 1 | Cab-O−Sil M5 | Cabot Corp. | | | ∼7.4 | 0.5 | 500 | TRIS buffer | |
| 2 | Cab-O−Sil M5 | | 203 | 6.70 | ∼7.4 | 0.1 | 100 | TRIS buffer | DPPC[a] |
| 3 | Cab-O−Sil M5 | | | | ∼7.4 | 0.1 | 100 | TRIS buffer | DPPC[b] |
| 4 | Zeosil Z45 | Rhodia Silica | 192 | 7.10 | ∼7.4 | 0.5 | 500 | TRIS buffer | |
| 5 | Zeosil Z45 | Systems | | | ∼7.4 | 0.1 | 100 | TRIS buffer | DPPC[b] |
| 6 | HDK T30[c] | Wacker Chemie | 305 | 4.47 | ∼7.4 | 0.6 | 500 | TRIS buffer | |
| 7 | HDK T40 | | 376 | 3.63 | 7.1−7.4 | 0.5 | 500 | NaCl solution | |

[a] Treated in an ultrasonic bath. [b] Treated with an ultrasonic tip. [c] Measurements done by Thron.[18]

## 2. Test Materials and Experimental Setup

The materials investigated are industrial products synthesized either by burning silicon tetrachloride in an oxygen−hydrogen flame[16] or by precipitating of saturated solutions. Table 1 summarizes the main properties of the silica and information regarding the experiments carried out. The synthetic amorphous form of silicon dioxide produced by flame pyrolysis is composed of so-called primary particles, which collide and are fused together to build up stable aggregates at the high flame temperatures.[17] Afterward, aggregates stick together to form loosely bonded agglomerates.[16] The high surface area observed (see Table 1) is not related to the occurrence of micropores, but can be attributed to the size of the primary particles.[17] These facts are confirmed by own nitrogen adsorption measurements which additionally show that Zeosil Z45 (precipitated) has also nearly no micropores. If we assume spherical geometry and uniform particle size the (average) particle radius can be calculated from the BET surface area which represents a measure for the size of the primary particles. This relationship represents a simple approximation and is used hereinafter, but the thermodynamic properties only depend on the size of these primary particles and not on the size and form of both the aggregates or agglomerates. Nevertheless, a distribution of the particle size is always present in real systems that are not in thermodynamic equilibrium.

Silica is dissolved under physiological conditions and osmotic pressure. The extracellular (lung) fluid is modeled by a physiological electrolyte. Thus, the dissolution experiments were carried out in a buffer solution (TRIS buffer)[19] of the following composition: 6.1 g of tris(hydroxymethyl)aminomethane; 35.4 mL of 1 N HCl solution, and 6.54 g of sodium chloride per liter. This solution provides comparable conditions in terms of pH, buffer capacity, and osmotic pressure (309 mosm/L) with respect to a physiological environment. The background electrolyte content (as sodium chloride) of the buffer solution is about 0.11 M. The application of TRIS buffer establishes the increasing velocity of dissolution with increasing ionic strength. To ensure reproducible results in determining the silica concentration only PMP flasks (poly(methylpentene)) and twice deionized water are employed. L-α-dipalmitoylphosphatidylcholine (Acros Organics) is used as the surface-active component. The standard silicate solution is prepared using a commercially available silicate standard solution for AAS (MERCK; 1000 mg/L). A 100 mL PMP flask is filled with 5 mL of this solution, 2.55 mL of 0.975 N HCl, and TRIS buffer solution. All other chemicals were of analytical purity grade.

For the dissolution experiment, a 500 mL PMP flask was filled with 0.5 g of silica and buffer solution (experiments 1−6; see Table 1) or sodium chloride solution (0.1 M; experiment 7). To prevent diffusion effects, the flask has been shaken at a constant temperature of 37 °C during the whole dissolution time. The pH and the total silica concentration were measured after defined times. In further experiments the surface active substance DPPC was added. Therefore, an amount of 25 mg of DPPC was given into 90 mL of the buffer solution and exposed to ultrasonic waves for about 2 h to yield a homogeneous suspension. To this suspension 0.1 g of silica was added and filled up to standard volume with buffer solution in a 100 mL flask. After this, it is treated as described above. The ultrasonic equipment used was the ultrasonic bath Brandelin Sonorex RK52 (experiment 2) and the ultrasonic tip Branson Sonofier (experiments 3 and 5). The total amount of dissolved silica is analytically determined by the molybdic acid method described by Motomizu et al.[20] Thereby, each data point is the average of four single determinations. For the determination of the silica concentration a volume of approximately 0.5−1 mL of the solution is withdrawn. The sample is filtered through a 0.2 $\mu$m syringe filter. Dynamic light scattering measurements of the filtered sample confirm a nearly complete removal of all particles. The solubility test of the different types of silica were performed twice to ensure reproducibility. A second analytical method (ICP−OES) was applied to determine the concentration of silica dissolved independent of possible disturbing effects arising from phosphate impurities. The measurements were carried out using a Maxim 112 manufactured by Fisons Instruments. The volume of the sample solution amounts to approximately 10 mL of the filtered solution. Additionally, a semiquantitative determination of the phosphorus content were undertaken with selected samples using ICP−OES. The undissolved solid of a whole flask is separated by centrifugation after a defined reaction time. Special solubility experiments had to be carried out, because a continuous determination of the silica concentration was not possible. The sample is dried after a washing procedure with water (repeated six times) to remove adsorbed molecules and ions, respectively. Afterward the specific BET[21] surface area is determined by nitrogen adsorption measurements at 77 K with the sorption automate AUTOSORB-1 of Quantachrome Corporation. First the sample is evacuated at 350 °C to remove the remaining water from the surface. The particle size is directly accessible by dynamic light scattering. These measurements have been accomplished with the ALV− NIBS/HPPS made by ALV GmbH. This device uses noninvasive backscattering for the determination of the particle size and the particle radius distribution.

## 3. Thermodynamic Model

For the theoretical description of the dissolution process of nanoparticles we have to look for a model which can describe the possible changes in these systems. All further theoretical relations are based on a proposal to model colloidal dispersion

thermodynamically which was suggested earlier.[15] This model represents further developments of considerations of phase transition.[22,23] For further details of the theoretical model see the literature cited.

All relations are derived for isothermal and isobaric conditions so that the Gibbs free energy is the natural potential function. The system is composed of two species, the colloid forming species (**1**) and the solvent (**2**). The state in which the colloid forming species is completely dissolved is used as the reference state. In all other possible states which can be formed from the whole amount of substance the colloid forming species is allowed to be distributed on the particle and the dissolved part, respectively. These states are compared to the reference state yielding the Gibbs free energy of colloid formation. Further on, a number of dimensionless quantities are introduced which are defined in eq 1.

$$\frac{\Delta_c g}{N_L^0(\mathbf{1}) k_B T} = g(r,z), \quad \frac{n_C^1(\mathbf{1})}{n_L^0(\mathbf{1})} = zr^3$$

$$z = \frac{Z}{N_L^0(\mathbf{1})}, \quad r = \frac{r_p}{r_0} \tag{1}$$

$$h = \frac{4\pi\sigma}{k_B T} r_0^{\,2} \quad a, b \ldots \text{constants}$$

Here, $k_B$ is the Boltzmann constant, $T$ is the temperature and $\sigma$ stands for the interfacial energy of silica/water using a value of 50 mN m$^{-1}$.[24] The amount of substance of the colloid forming species (**1**) contained in the nanoparticles, $n_C^1(\mathbf{1})$, is related to the whole amount of substance of species **1**, $n_L^0(\mathbf{1})$, yielding a dimensionless quantity. Therefore, the number of particles, $Z$, is related to the total number of molecules of species **1**, $N^0{}_L(\mathbf{1})$, whereas the radius of the particle, $r_p$, is related to the radius of a molecule, $r_0$. The parameter $h$ represents the surface term whereas $a$ and $b$ are constants. Introducing the supersaturation, $y = n^0{}_L(\mathbf{1})/n_L^s(\mathbf{1})$, as the quotient of $n^0{}_L(\mathbf{1})$ and the amount of species **1** in the saturated solution, $n_L^s(\mathbf{1})$, the dimensionless Gibbs free energy of colloid formation as a function of cluster size ($r$) and cluster concentration ($z$) can now be written as

$$g(r,z) = (1 - zr^3)\ln(y(1 - zr^3)) - \frac{1}{a}(1 - azr^3)$$
$$\ln(1 - azr^3) + hzr^2 - zr^3 \ln b - \ln y \tag{2}$$

The surface belonging to the expression in eq 2 can be calculated for a specific initial supersaturation. The corresponding part of $g(r, z)$ is shown in Figure 1 allowing us to see the main properties of the potential function. The calculations are carried out for the dissolution experiment with Cab−O−Sil M5, thus the supersaturation and the temperature are selected as in the experiment ($y = 8.32$, $T = 310.15$ K). All drawn curves are described in detail in the caption of Figure 1.

## 4. Kinetic Model and Numerical Calculations

Changes of the actual system should occur along the steepest slope of the potential function. This behavior is described by the gradient at any point of the surface. The gradient, $\nabla g(r, z)$, can be written as

$$\nabla g(r,z) = \left(\frac{\partial g(r,z)}{\partial r}\right)_z \vec{e}_r + \left(\frac{\partial g(r,z)}{\partial z}\right)_r \vec{e}_z \tag{3}$$

$\vec{e}_r$ and $\vec{e}_z$ represent the unit-vectors in $r$- and $z$-directions, respectively. The path of a system starting at any point at the surface is obtained by simple geometric considerations[22] and can be written in the form

$$\frac{dz}{dr} = \frac{\left(\frac{\partial g(r,z)}{\partial z}\right)_r}{\left(\frac{\partial g(r,z)}{\partial r}\right)_z} = \frac{r\left[-\ln\left(\frac{yb(1 - zr^3)}{1 - azr^3}\right) + \frac{h}{r}\right]}{3z\left[-\ln\left(\frac{yb(1 - zr^3)}{1 - azr^3}\right) + \frac{2h}{3r}\right]} \tag{4}$$

These gradient curves need to be determined by numerical methods. The curve of the development of the system can be predicted point by point—beginning with a defined starting point. This starting point is determined by the total mass and the mean size of the particles exposed to dissolution. In Figure 2, the broken line starting at point $P$ is determined in such a way. For the dimensionless quantities $r$ and $z$, respectively, only exists the relation $z(P)r^3(P) = 1$ in the initial state if nothing is dissolved which is indicated by the point $P$ in Figure 2. The initial particle radius, $r(P)$, can be calculated using the relations in eq 5 after obtaining the average particle radius, $r_p^{avg}$, by nitrogen adsorption measurements.

$$r_p^{avg} = \frac{3}{S_{BET}\rho_p}$$

$$r(P) = \frac{r_p^{avg}}{r_0} = \frac{3}{S_{BET}\rho_p r_0} \tag{5}$$

In eq 5 $\rho_p$ is the density of a particle, which is assumed to be equal to the density of $SiO_2$ with a value of $\rho_{SiO_2} = 2.2$ g/cm$^3$.

Furthermore, the kinetic aspects must be involved. The knowledge of changes over time is very important besides describing the way of the developments of the systems. A simple approach can be gained from the properties of the potential function. It is assumed that the time required between two states is inversely proportional to the gradient of the potential function. Strong changes of the gradient cause short transition times. If the differences in Gibbs free energy are large, the changes in the system proceed even quicker. For this reason, we suggest a rate law using a simple linear relation. This dependence can now be written as

$$\frac{dc_L^1(1)}{dt} = -kB(c_L^1(1))|\nabla g(r,z)| \tag{6}$$

The factor $B(c_L^1(1))$ depends on the actual silica concentration, $c_L^1(1)$ ($c_L^1 = c_s$). In conclusion, the concentration−time curve of dissolution is accessible from thermodynamic and kinetic considerations. Our experimental measurements are adapted to the model obtaining the rate constant, $k$, of the dissolution process. All numerical calculations as well as the nonlinear fit were carried out with the software *Mathematica*.[25]

The fitting procedure is done as followed: The differential eq 4 is calculated for the corresponding parameters of the dissolution experiment beginning with the point, where the whole silica is contained in particles of uniform size (point $P$ in Figure 2). The radius is calculated after eq 5 from nitrogen adsorption measurements. This numerical calculation is carried out up to the point, where the actual cluster concentration in the system has reached ~0.5% of its initial value. Because of difficulties in the numerical calculations (step width, numerical precision of intermediate data), this end point was established

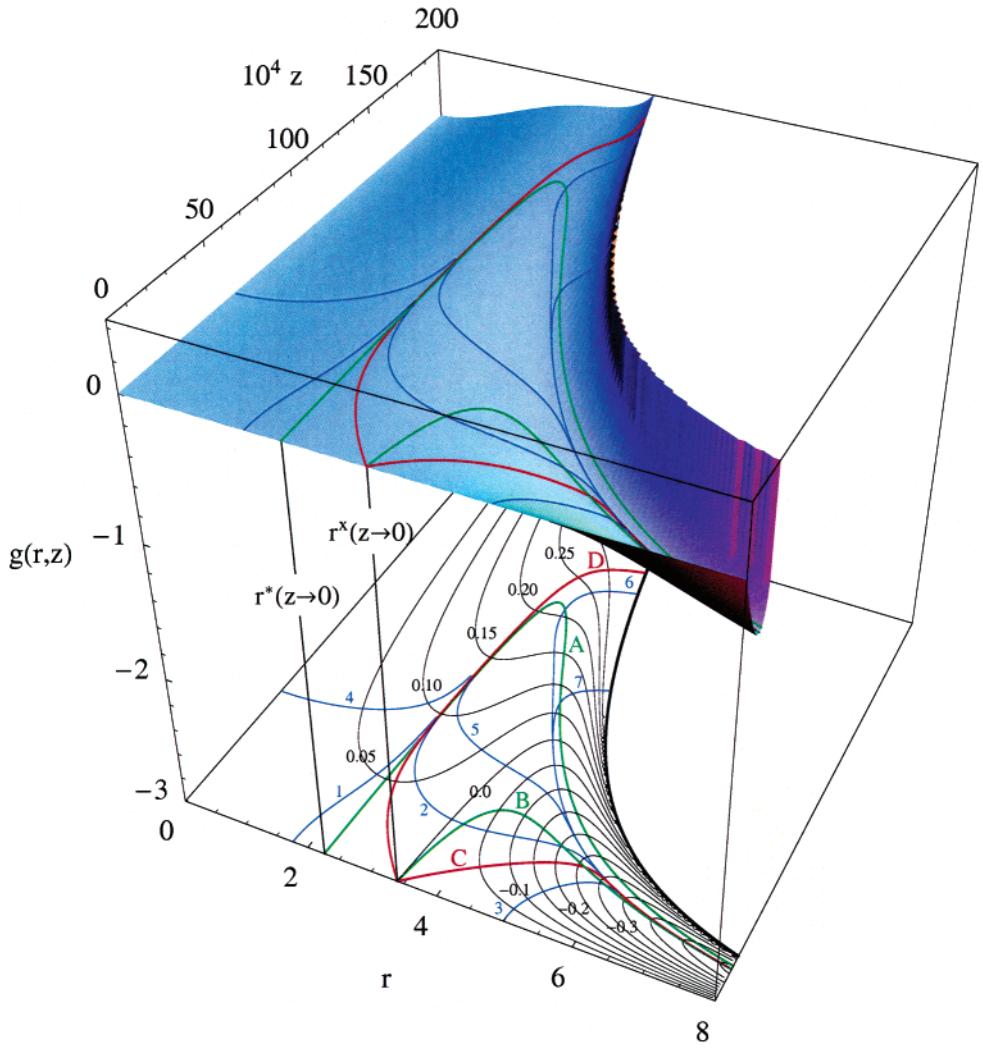


**Figure 1.** Surface of Gibbs free energy of cluster formation, $g(r, z)$, as a function of cluster size, $r$, and cluster concentration, $z$, calculated for silica particles with $y = 8.32$ and $T = 310.15$ K. The green curves are the partial derivatives of $g(r, z)$ respecting $r$ (A) and $z$ (B), respectively. Further graphs, containing two red lines and seven blue lines labeled with the corresponding numbers, indicate the strongest change of the potential function determined by the discussed gradient curve (eq 4). Red line C fixes the bottom of the valley of $g(r, z)$ whereas the two blue lines 6 and 7 stand as examples for development of a dissolution system.

for all calculations. The rate law has to be separated into a time depending and a concentration depending part, whereas both parts must be equal to the same constant $m$:

$$\frac{\mathrm{d}c_{\mathrm{L}}^{1}(1)}{B(c_{\mathrm{L}}^{1}(1))} = m = -k|\nabla g(r, z)|\,\mathrm{d}t \tag{6a}$$

Both parts can be obtained by the numerical integration by solving eq 7a and eq 7b.

$$c_{\mathrm{L}}^{1}(\mathbf{1}) = m\int_{\xi=\xi_0}^{\xi} B(\xi)\,\mathrm{d}\xi \tag{7a}$$

$$t = -\frac{m}{k}\int_{\xi=\xi_0}^{\xi} \frac{\mathrm{d}\xi}{|\nabla g(r, z)|} \tag{7b}$$

Here, $\xi$ stands for $r$ or $z$, respectively. The silica concentration as a function of dissolution time can be obtained connecting the eqs 7a and 7b in the following form:

$$c_{\mathrm{L}}^{1}(\mathbf{1}) = -kt\frac{\int_{\xi=\xi_0}^{\xi} B(\xi)\,\mathrm{d}\xi}{\int_{\xi=\xi_0}^{\xi} \frac{\mathrm{d}\xi}{|\nabla g(r, z)|}} \tag{8}$$

The combined time depending concentration is fitted to the experimental data by nonlinear regression, yielding a rate constant for the dissolution process as only parameter.

## 5. Experimental Results

The experiments can be divided into two groups. First, the solubility test was carried out without any surface active substance. And second, DPPC was added after it was exposed to ultrasonic waves. A summary of the solubility systems investigated and the measured quantities is listed in Table 1. At the chosen ratio of the mass of silica and the volume of solvent the supersaturation is always $y = 8.32$ in all experiments. Only in the dissolution experiment with HDK T30[18] (experiment 6) is the supersaturation slightly higher ($y = 9.99$). Therefore, the experiments can be compared with each other with only a few restrictions.

The pH in the dissolution experiments carried out in buffer solution is constant over the whole dissolution time, which could be proven by own measurements. In experiment 7 with HDK T40 the buffer solution has been substituted by an aqueous sodium chloride solution of approximately the same background electrolyte concentration. This system of comparison should serve to investigate the surface morphology of samples of the

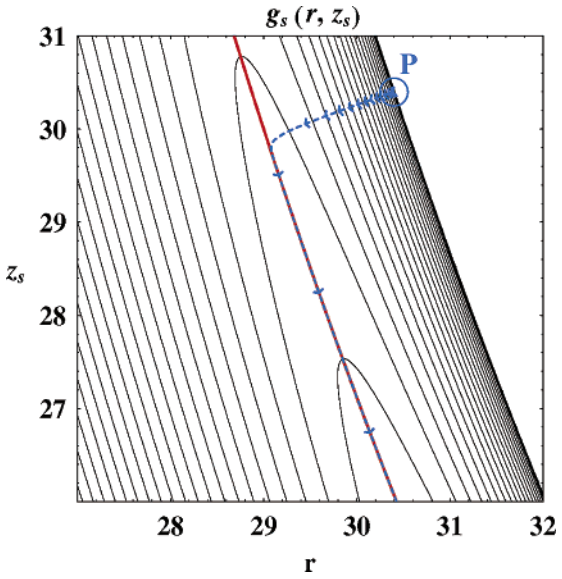


**Figure 2.** Corresponding section of the contour plot of the Gibbs free energy calculated for the dissolution of Cab−O−Sil M5 ($T = 310.15$ K; $y = 8.32$) after scaling the ordinate to have the same numerical value as the abscissa in point *P*. The starting point of the dissolution process is indicated by the point labeled *P* (open circle). The broken blue line is the calculated gradient curve after eq 4 and the red line indicates the bottom of the valley.

**TABLE 2: Maximum Silica Concentration Observed, $c^1_{L,max}$(1), as a Function of the Primary Particle Radius, $r_p^{avg}$, Obtained by Nitrogen Adsorption Measurements (eq 5)**

| silica | $r_p^{avg}$ (nm) | $c^1_{L,max}$(1) (mmol/L) |
|---|---|---|
| Zeosil Z45 | 7.13 | 2.30 |
| Cab-O-Sil M5 | 6.73 | 2.35 |
| HDK T30 | 4.49 | 2.55 |
| HDK T40 | 3.64 | 2.70 |

dissolution experiment without the disturbing effect of the buffer component tris(hydroxymethyl)aminomethane. In this case, the pH value slightly decreased during the dissolution from its starting value of 7.4 to a value of 7.1 after 3 months of dissolution. The repeated adjustment of the pH value was not carried out because of the relatively small changes.

**Solubility of Amorphous Silica.** First off all the dissolution experiments were carried out without any surface active component. The dissolution behavior of the four different silica without addition of the surface active component are shown in the four diagrams A−D in Figure 3. Thereby, the actual silica concentration, $c_S$, is plotted against the dissolution time. The black line in each of the figures represents the theoretical dissolution curve after fitting at the experimental data. Additionally, the confidence intervals (95%) from the nonlinear regression procedure are indicated by the broken black lines.

In all cases, the silica concentration, $c_S$, rises very quickly and exceeds the saturation concentration of the bulk phase, which can be assumed to be 2 mmol/L at 25 °C.[24] Differences between the dissolution experiments of all samples can be found in the temporal development and the reached maximum silica concentration. Here, the experimental results are in accordance with the theoretical model. The maximum silica concentration observed depends on the primary particle radius, which is listed in Table 2. If the radius of silica particles decrease a higher silica concentration can be observed. This correlation is predicted by the described model and is an analogue to the well-known Kelvin effect. Thus, the fitted curves show a very good agreement with the experimental data.

As expected, the highest silica concentration is observed in the dissolution experiment with HDK T40. This experiment was in fact carried out in aqueous sodium chloride solution instead of buffer solution but shows the expected behavior. In principle, the dissolution process of these nanodispersed silica can be subdivided into two parts. During the first phase monomeric units have to be displaced from the particle surface yielding the initial concentration of dissolved silicic acid. This process runs very quickly and causes a strong increase of the silica concentration. In the course of this process the strongly curved surface of the nanoparticles leads to a distinct higher concentration as expected for a bulk phase with a plane surface. At the same time, where the concentration increases, the average particle radius has to decrease due to the displaced monomeric units. This causes the observable maximum. After this, another effect appears in the further course of the dissolution process. In the second phase, the average particle radius increases, but the concentration is now reduced. We explain it with the beginning of the precipitation of monomeric units from the solution onto the particle surface. This process is known as Ostwald ripening. The amorphous bulk phase with a plane surface should be reached at the end of this process, which stands in contact to a saturated solution. All experimental data more or less show this behavior, but do not reach this point after three months of dissolution.

**Influence of Surfactant.** In further experiments, 25 mg of DPPC was added into 100 mL of solution as described in the Experimental Section. This procedure ensures similar conditions which are found in biological lung fluid. Here, we are interested in a possible influence of the surface active component on the dissolution process. The experiments with two silica were repeated under these special conditions whereas the experiment with Cab-O-Sil M5 were performed exposing the surfactant to both methods of ultrasonic treatment. The three diagrams E−G in Figure 4 show the experimental obtained dissolution data and the corresponding to theoretical curve. The dissolution behavior observed is quite similar to that obtained without addition of the surfactant. A small effect of DPPC on the dissolution kinetics could be indicated by comparison of Figures 3 and 4. In the case of experiments 2 and 3 there exist only few deviations to the corresponding experiment 1. It seems, that the silica concentration is slightly higher by adding DPPC to the system at longer dissolution times. This effect appears in experiment 5, too, where the dissolution seems to be decelerated in comparison to experiment 4. This context is confirmed if we adapt our measurements to our model proposed, because the rate constant obtained (Table 3) is smaller by a factor of 3, approximately, for the dissolution experiment with addition of DPPC when compared to the experiment of the same silica (Zeosil Z45) where no surfactant was added (experiment 4).

**ICP—OES Measurements.** As soon as the solution contains phosphate, the molybdic acid method is no longer suitable to determine the silica concentration. The ICP−OES represents an excellent method both to validate the molybdic acid method and to investigate the influence of a possible phosphate (phosphorus) content in the sample solution. During the dissolution experiment of Cab-O-Sil M5 (1 and 2), the silica concentration was determined by both methods. Figure 5 shows the results of this investigation. The figure shows the concentration obtained by the molybdic acid method (diamonds with error bars) and the ICP−OES measurements for Si in the case of experiment 2. With both methods, comparable silica concentrations are obtained as was observed in the experiment without addition of the surfactant, too. This fact is confirmed by the

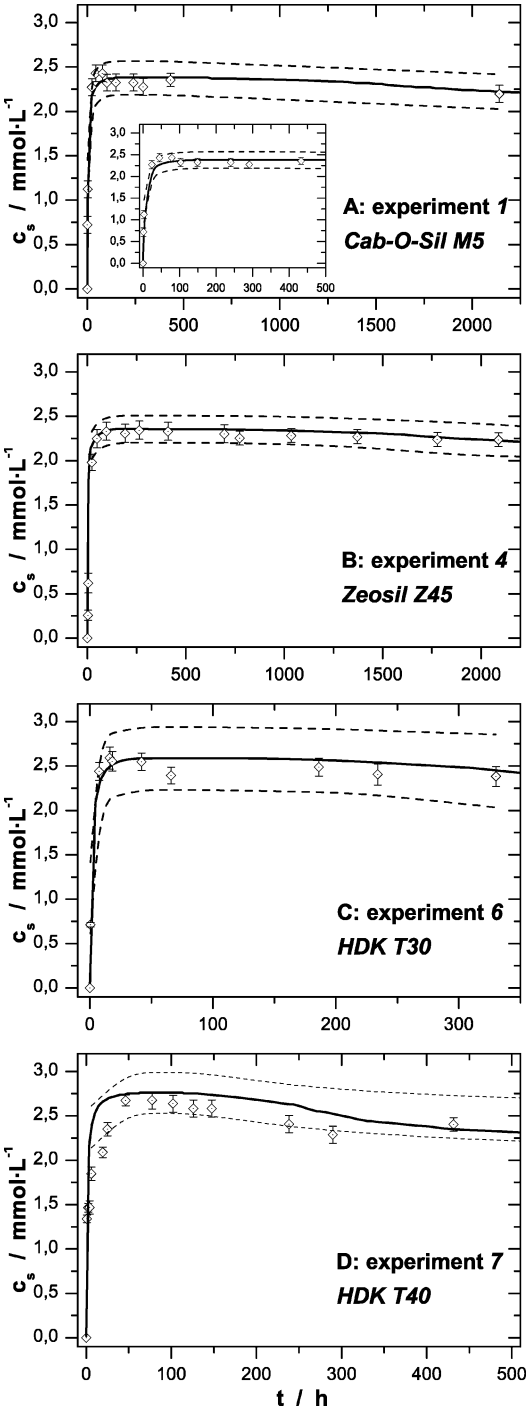


**Figure 3.** Dissolution behavior of the dissolution experiments 1, 4, 6, and 7 (graph A to D) without addition of the surfactant at 37 °C. Measurements are represented by the diamonds with the corresponding error bar. In each diagram, the black lines represent the results of the nonlinear regression of our dissolution model with the confidence intervals (95%; broken lines).

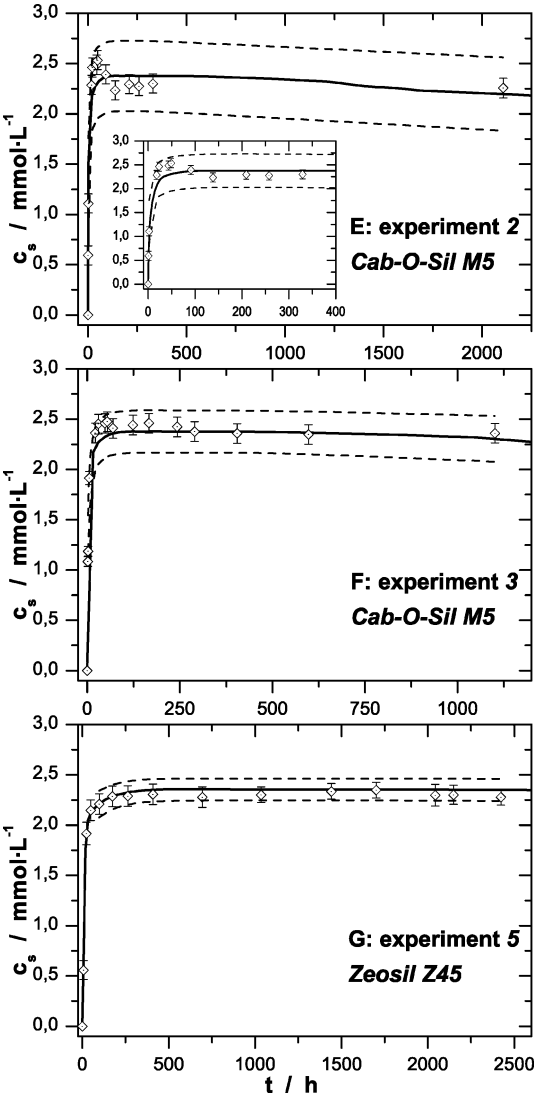


**Figure 4.** Effect of the surface active substance DPPC on the solubility behavior of Cab-O-Sil M5 and Zeosil Z45 at 37 °C. A total of 25 mg of the surfactant is dispersed in the solvent and treated with an ultrasonic bath (E) or and ultrasonic tip (F and G) for 2 h before adding the silica.

**TABLE 3: Kinetic Constants of the Different Solubility Experiments Obtained by Fitting to the Theoretical Model**

| | | rate constant | | |
|---|---|---|---|---|
| no. | dissolution experiment with silica | $k^a$ ($h^{-1}$) | $k_+{}^b$ (mol $m^{-2}$ $s^{-1}$) | corr coeff $R$ |
| 1 | Cab-O-Sil M5 | $2.89 \times 10^{-7}$ | $7.88 \times 10^{-13}$ | 0.976 |
| 2 | Cab-O-Sil M5 | $2.42 \times 10^{-7}$ | $3.30 \times 10^{-12}$ | 0.915 |
| 3 | Cab-O-Sil M5 | $2.06 \times 10^{-7}$ | $2.82 \times 10^{-12}$ | 0.960 |
| 4 | Zeosil Z45 | $6.88 \times 10^{-7}$ | $1.99 \times 10^{-12}$ | 0.939 |
| 5 | Zeosil Z45 | $2.16 \times 10^{-7}$ | $3.13 \times 10^{-12}$ | 0.993 |
| 6 | HDK T30 | $6.62 \times 10^{-7}$ | $1.00 \times 10^{-12}$ | 0.966 |
| 7 | HDK T40 | $8.05 \times 10^{-6}$ | $2.57 \times 10^{-12}$ | 0.913 |

[a] Results of the numerical calculations. [b] Related to initial surface area.

results of the determination of the phosphorus content. There is no measurable phosphorus content in all investigated sample solutions from the dissolution experiments. Therefore, phosphate from DPPC is not going into the solution even after the mentioned ultrasonic treatment of the surface active component DPPC. This statement is for the above-mentioned ultrasonic treatment with adequate cooling of the sample solution and has to be proven for every kind of sample preparation. Additionally, in the chemicals used in our experiments like twice deionized water and so on, no silicate or phosphate contamination can be found with ICP−OES. As a result, the determination of the silica concentration can be performed without any restriction by the molybdic acid method.

**Surface Area.** Our theoretical model predicts significant changes in the particle geometry during the dissolution. In the first step, the average particle radius has to decrease due to the initial dissolution process whereas it growths in further time because of the Ostwald ripening of the particles. These processes

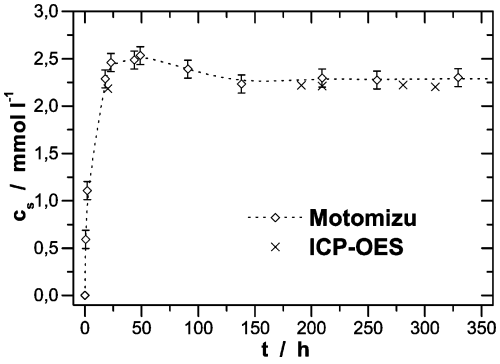


**Figure 5.** Comparison between both methods for determining silica concentration in the dissolution experiment 2. Open diamonds indicate the result determined with the method of Motomizu whereas crosses represent ICP−OES measurements.

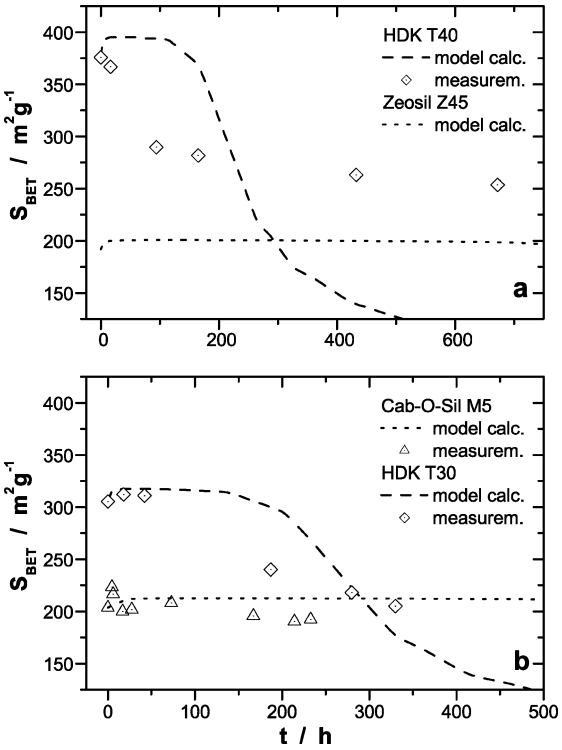


**Figure 6.** Experimental data and theoretical prediction of the development of specific surface area, $S_{BET}$, as a function of dissolution time.

lead to changes in the surface morphology and thus in the specific surface area. Without an additional fitting procedure the temporal development of the specific surface area, $S_{BET}$, determinable by the BET method,[21] with nitrogen adsorption measurements can be predicted. Figure 6 shows the theoretical course of the specific surface area, $S_{BET}$, for the dissolution experiments of all silica samples without surfactant. In the case of experiment 6 (HDK T30) the theoretical course as well as the measurements very well agree with each other. Instead of this, the theoretical predictions only represent the trend in the surface areas measured in the other experiments. This fact could be caused by the great number of wash processes needed before nitrogen adsorption measurements. Each washing process represents a new dissolution experiment and causes significant changes in the surface morphology therefore. Another possibility is to use the specific surface areas measured after the dissolution for the determination of the best fit. In this case the kinetic constant would be no longer a free parameter.

**Light Scattering.** As already mentioned, the primary objective of dynamic light scattering measurements (following the development of particle size during the dissolution) could not be reached. This is caused by the fact that there has been no success in destroying the aggregates of silica in general in order to determine the primary particle size directly. A possible reason is the high stability of the aggregates formed at the high flame temperature during the production process.[16] These aggregates cannot be destroyed by the applied ultrasonic methods. So, we only measure the hydrodynamic radius of an aggregate or agglomerate assuming spherical geometry. Besides this, the method is very well suited to determine the particle radius distribution of DPPC-dispersions. In dependence on the kind of the ultrasonic treatments and elapsed time, one can assess which method leads to the best results. The time-dependent development of the particle size distribution of DPPC dispersions is shown in Figure 7. A difference between both methods can clearly be recognized. Applying the ultrasonic tip, particle size distributions are obtained, which are clearly shifted to smaller values of particle radius (full black line) when compared to the other method with the ultrasonic bath (broken black lines in Figure 7). A more exact inspection shows a shift of the maximum in the range of one decimal order. Therefore, the ultrasonic tip (Branson Sonofier) is the more efficient device in destroying larger agglomerates. Nevertheless, a molecular distribution of the surfactant cannot be obtained by the ultrasonic treatment. In conclusion, a possible influence of DPPC on the dissolution process of silica cannot ultimately be excluded for the case where a noticeable smaller particle size distribution or molecular distribution is obtained. Additionally, the investigations allow us to confirm that the filtration of the sample solutions with a syringe filter is suitable to (nearly) remove all particles dispersed. Such a filtered solution, no matter if DPPC is added or not in the dissolution experiment, shows a light

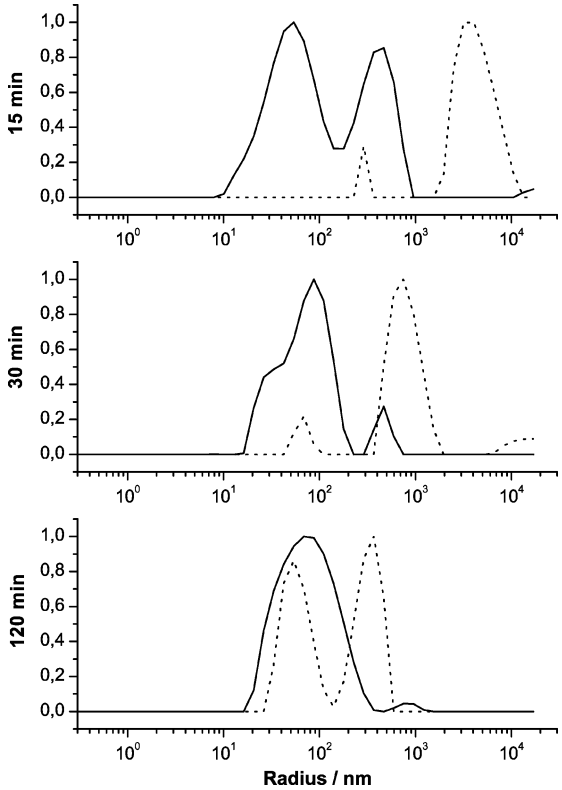


**Figure 7.** Particle radius distribution of DPPC suspensions (25 mg per 100 mL buffer solution) after different time of ultrasonic treatment applying the ultrasonic treatment with the ultrasonic tip (full black lines) or the ultrasonic bath (broken black lines).

scattering behavior similar to that of a blank sample of buffer solution.

## 6. Results

Table 3 shows the values of the determined rate constants for the dissolution experiments. These results are obtained by applying eq 8 with the above-mentioned numerical calculations. On the basis of the described problems in numerical computation, this procedure can only be accomplished with some restrictions. At present, the different kinetic constants cannot be compared with each other because of the mentioned problems. However, the agreement between the experimental data and the theoretical adaptation is very good. The differences in the maximum of the silica concentration observed as well as the common dissolution behavior can be very well predicted by the proposed model. Our overall rate constants, $k_+$, determined are of similar orders of magnitude when compared to the results of Icenhower et al.[4] and Vogelsberger et al.[5] The specific surface area measured at the beginning of the dissolution experiment is used for the calculation of $k_+$. As we have shown the specific surface area changes during the dissolution experiment especially in the case where nanoparticles are used. Therefore the preference should be to give the rate constant in units of reciprocal time in all cases where the dissolution of very small particles is investigated. The interpretation of the rate constant can also be done by a kinetic model described in the refs 26 and 27. The model contains contributions of elementary dissolution reactions of uncharged and negatively and positively monocharged surface species. The influence of the pH value and the ionic strength are described well. The plateau values of the dissolution curves can be interpreted as equilibrium saturation concentrations of the actual particle sizes present in the solution. The really stable state of the dissolution system is the equilibrium of the bulk silica having a plane surface. It will be obtained from the systems with small particles by Ostwald ripening. Vogelsberger et al.[5] have investigated and calculated the temperature dependence of the saturation concentration for different temperatures (25, 45, and 55 °C). Our experimental data show a similar behavior, so that the saturation concentration of amorphous silica at 37 °C is higher than the 2 mmol/L that we have assumed.

The temporal course of the specific surface area is already defined by the adaptation of the concentration−time course. No additional fitting procedure is necessary, and it was not carried out for this reason. The surface areas show an interesting characteristic which can be seen in Figure 6. At the beginning of the dissolution process monomeric units are displaced from the particle surface to yield the initial silica concentration. This process associates a lowering of the particle radius and therefore, an increase of the specific surface area at the same time. All theoretical curves show this behavior. In the case of HDK T30, the initial increase was observed in the measurements, too. In the other cases, the preceding washing procedure prevents a simple interpretation of the experimental measurements, because every wash process represents a new dissolution experiment. In the further dissolution process, the surface areas decrease, which is the same as an increased particle radius. This development strengthens the assumption of the Ostwald ripening of the particles.

## 7. Discussion

The solubility behavior of technical produced silicas has been investigated in the present work. The environment of the dissolution was adapted to physiological media such as extracellular fluid.

The dissolution of different technical silica was investigated in TRIS buffer solution and in aqueous sodium chloride solution, respectively. In general, the silica concentration strongly increases up to its maximum value at first. This maximum clearly exceeds the value of the saturation concentration of bulk amorphous $SiO_2$ of 2.0 mmol $L^{-1}$ at 25°C. Of course, the dissolution temperature chosen (37 °C) has a small contribution to the maximum silica concentration observed. But, the maximum silica concentrations of 2.30−2.70 mmol/L obtained in the experiments clearly depend on the particle radii. It is confirmed by our theoretical model proposed which considers the size effect of nanoparticles. After reaching the maximum, the silica concentration slowly decreases. This can be attributed to the Ostwald ripening of the particles. The concentration does not attain the saturation values even after 3 months of dissolution. In the case of HDK T40, where no buffer was used, the pH can also be assumed to be nearly constant over the whole dissolution time. In general, the observed differences between the solubility experiments are caused by different particle size. In the second part of the investigations, the system silica−TRIS buffer was further adapted to get closer to the conditions, which can be found in the extracellular lung fluid. The added surface active compound DPPC had to be dispersed by ultrasonic treatment. This is necessary to achieve a homogeneous suspension, which does not tend to form larger aggregations. It was shown, with the dynamic light scattering, that the second treatment (ultrasonic tip) is the more efficient method for destroying the aggregations. In the case of Cab-O-Sil M5, only a slight difference between the solubility experiments without and with addition of surfactant was observed. Similar results were obtained by observing the dissolution behavior of Zeosil Z45 under the same conditions. In general, if the surface active part is added, the dissolution process seemed to be slightly decelerated when compared to the experiment without addition. However, it has to be established by further experiments. A chemical reaction between components of the TRIS buffer and DPPC has not been observed but cannot be excluded in general.

The described thermodynamic model is very well suitable for the description of such kind of colloidal dispersion. The theoretically calculated curves show a very good agreement with the experimental data. So, we can fit a free parameter for each solubility experiment which can be understood as the rate constant of the dissolution process.

The problem of the preceding washing procedure prevents a simple interpretation of the measurements of the specific surface areas with nitrogen adsorption. The washing procedure, which is needed to remove any adsorbed molecules or ions from the surface, has a significant influence on the results of surface area measurements. This disturbing influence depends on the washing solvent and the number of washing procedures.[28] Due to this fact, the observed development of the specific BET-surface areas only shows the expected trend but does not represent the exact values with great probability. Here, special experiments have to be carried out to investigate the changes of the surface morphology in more detail. Then, another variable which is accessible experimentally can ensure our theoretical model.

As a result of our experimental and theoretical investigations, we can conclude that nanosized silica particles show an increased solubility. The existence of special surface active components (surfactant) does not show a significant influence on the dissolution behavior of such type of silica in biological-like media. Furthermore, the increased energy of these nano-

particles compared to the bulk phases is responsible for a relatively fast dissolution process and higher maximum silica concentrations observably. Small amounts of nanosized silica particles should be quickly dissolved in a biological environment such as extracellular lung fluid.

**Acknowledgment.** We thank the Association of Synthetic Amorphous Silica Producers (ASASP) for financial support of this work.

## References and Notes

(1) Mattson, S. M. *Ann. Occup. Hyg.* **1994**, *38*, 857.
(2) Thélohan, S.; de Meringo, A. *Environ. Health Perspect. Suppl.* **1994**, *102* (5), 91.
(3) Lehuédé, P.; de Meringo, A.; Bernstein, D. M. *Inhal. Toxicol.* **1997**, *9*, 495.
(4) Icenhower, J. P.; Dove, P. M. *Geochim. Cosmochim. Acta* **2000**, *64*, 4193.
(5) Vogelsberger, W.; Mittelbach, T.; Seidel, A. *Ber. Bunsen-Ges. Phys. Chem.* **1996**, *100*, 1118.
(6) House, W. A.; Denison, F. H.; Warwick, M. S.; Zhmud, B. V. *Appl. Geochem.* **2000**, *15*, 425.
(7) Zhmud, B. V.; House, W. A.; Denison, F. H. *J. Chem. Soc., Faraday Trans.* **1997**, *93*, 3473.
(8) Ding, J.; Doudevski, I.; Warriner, H. E.; Alig, T.; Zasadzinski, J. A.; Waring, A. J.; Sherman, M. A. *Langmuir* **2003**, *19*, 1539.
(9) Frosolono, M. F.; Charms, B. L.; Pawlowski, R.; Slivka, S. *J. Lipid. Res.* **1970**, *11*, 439.
(10) Hills, B. A. *J. Appl. Physiol.* **1999**, *87*, 1567.
(11) Ingenito, E. P.; Mark, L.; Morris, J.; Espinosa, F. F.; Kamm, R. D.; Johnson, M. *J. Appl. Physiol.* **1999**, *86*, 1702.
(12) Wright, S. M.; Hockey, P. M.; Enhorning, G.; Strong, P.; Reid, K. B. M.; Holgate, S. T.; Djukanovic, R.; Postle, A. A. *J. Appl. Physiol.* **2000**, *89*, 1283.
(13) Bernhard, W.; Hoffmann, S.; Dombrowsky, H.; Rau, G. A.; Kamlage, A.; Kappler, M.; Haitsma, J. J.; Freihorst, J.; von der Hardt; H.; Poets, C. F. *Am. J. Respir. Cell Mol. Biol.* **2001**, *25*, 725.
(14) Kaushal, S.; Ghosh, S.; Sharma, N.; Sanyal, S. N.; Majumdar, S. *Cell. Mol. Life Sci.* **2001**, *58*, 2098.
(15) Vogelsberger, W. *J. Phys. Chem. B* **2003**, *107*, 9669.
(16) Barthel, H.; Heinemann, M.; Stintz, M.; Wessely, B. *Chem. Eng. Technol.* **1998**, *21*, 745.
(17) Barthel, H.; Rösch, L.; Weis, J. Fumed Silica—Production, Properties, and Applications. In *Organosilicon Chemistry II: Form Molecules to Materials*; Auner, N., Weis, J., Eds.; VCH: Weinheim, Germany, 1996; p 761.
(18) Thron, D. Diploma Thesis, F.-Schiller-University, Jena, Germany, 2001.
(19) Zander, R. Patent No. DE 3321200 A1, 1984.
(20) Motomizu, S.; Oshima, M.; Ojima, Y. *Anal. Sci.* **1989**, *5*, 85.
(21) Brunauer, S.; Emmett, P. H.; Teller, E. *J. Am. Chem. Soc.* **1938**, *60*, 309.
(22) Vogelsberger, W.; Beck, M.; Fritsche, M.; Mäurer, F. *Z. Phys. Chem., Neue Folge* **1992**, *175*, 201.
(23) Vogelsberger, W. *Z. Phys. Chem.* **2001**, *215*, 1099.
(24) Iler, R. K. *The Chemistry of Silica*; J. Wiley & Sons: New York, 1979; p 54.
(25) Wolfram, S. *Das Mathematica Buch*, 3. Auflage; Addison-Wesley-Longman: Bonn, Germany, and Paris, 1997.
(26) Löbbus, M.; Vogelsberger, W.; Sonnefeld, J.; Seidel, A. *Langmuir* **1998**, *14*, 4386.
(27) Vogelsberger, W.; Seidel, A.; Breyer, T. *Langmuir* **2002**, *18*, 3027.
(28) Roelofs, F. Diploma Thesis, F.-Schiller-University, Jena, Germany, 2002.